FEBS openbio

FEBS PRESS science publishing by scientists

Structural enzymology comparisons of multifunctional enzyme, type-1 (MFE1): the flexibility of its dehydrogenase part

Prasad Kasaragod[1], Getnet B. Midekessa[1], Shruthi Sridhar[1], Werner Schmitz[2], Tiila-Riikka Kiema[1], Jukka K. Hiltunen[1] and Rik K. Wierenga[1]

1 Biocenter Oulu and Faculty of Biochemistry and Molecular Medicine, University of Oulu, Finland
2 Theodor Boveri Institute of Biosciences (Biocenter), University of Würzburg, Germany

Keywords
CoA; crotonase; dehydrogenase; NAD; substrate channeling

Correspondence
R. K. Wierenga, Biocenter Oulu and Faculty of Biochemistry and Molecular Medicine, University of Oulu, PO Box 5400, FI-90014 Oulu, Finland
Fax: +358 8 344 084
Tel: +358 2 94481199
E-mail: rik.wierenga@oulu.fi

(Received 4 October 2017, revised 13 October 2017, accepted 14 October 2017)

doi:10.1002/2211-5463.12337

Multifunctional enzyme, type-1 (MFE1) is a monomeric enzyme with a 2E-enoyl-CoA hydratase and a 3S-hydroxyacyl-CoA dehydrogenase (HAD) active site. Enzyme kinetic data of rat peroxisomal MFE1 show that the catalytic efficiencies for converting the short-chain substrate 2E-butenoyl-CoA into acetoacetyl-CoA are much lower when compared with those of the homologous monofunctional enzymes. The mode of binding of acetoacetyl-CoA (to the hydratase active site) and the very similar mode of binding of NAD^+ and NADH (to the HAD part) are described and compared with those of their monofunctional counterparts. Structural comparisons suggest that the conformational flexibility of the HAD and hydratase parts of MFE1 are correlated. The possible importance of the conformational flexibility of MFE1 for its biocatalytic properties is discussed.

Database
Structural data are available in PDB database under the accession number 5MGB.

In higher eukaryotes, the fatty acid degradation by β-oxidation is located in peroxisomes [1–3] as well as in mitochondria [4–6]. The peroxisomal β-oxidation pathway catalyzes the degradation of the very long straight chain, 2-methyl branched chain, as well as bile acid intermediates and polyunsaturated fatty acid chains, whereas the mitochondrial β-oxidation degrades predominantly the saturated, long-, medium-, and short-chain fatty acids. Peroxisomal β-oxidation is catalyzed by monofunctional and multifunctional enzymes. The first step of the peroxisomal β-oxidation pathway (Fig. 1), the acyl-CoA oxidase reaction, and the fourth (last) step, the thiolase reaction, are catalyzed by monofunctional enzymes. The peroxisomal multifunctional enzyme, type-1 (MFE1) catalyzes the second and third steps. MFE1 is a monomeric enzyme [7]. The N-terminal region catalyzes the second step of β-oxidation, which is the hydratase reaction (EC 4.2.1.17), as well as the Δ^3,Δ^2-enoyl-CoA isomerase reaction (EC 5.3.3.8) [8,9]. The third step of the β-oxidation pathway, the NAD-dependent dehydrogenation reaction of 3-hydroxyacyl-CoA (EC 1.1.1.35), is catalyzed by the C-terminal part of MFE1. MFE1 is also known as the L-bifunctional protein, because of the chirality of the 3-hydroxy intermediate, being 3S-hydroxyacyl-CoA [10]. MFE1 has been proposed to play a key role in the metabolism of dicarboxylic fatty acids [11,12]. MFE1 is one of the most abundant enzymes in mammalian peroxisomes; nevertheless, MFE1 deficiency diseases have not yet been described, suggesting that

Abbreviations
AcAc-CoA, acetoacetyl-CoA; HAD, 3S-hydroxyacyl-CoA dehydrogenase; HsHAD, the human, mitochondrial, dimeric, monofunctional HAD; MES, 2-(N-morpholino) ethanesulfonic acid; MFE1, multifunctional enzyme, type-1; PIPES, piperazine-N,N′-bis(2-ethanesulfonic acid); rpMFE1, the rat, peroxisomal, monomeric MFE1; Tris, tris(hydroxymethyl)-aminomethane.

MFE1 is important under as of yet uncharacterized metabolic stress.

Substrate specificity studies have shown that MFE1 can catalyze the hydration of long-chain linear acyl chains as well as of the bulky bile acid intermediates. The latter acyl moieties also have a 2-methyl group. Interestingly, the chiral specificity for the 2-methyl group is different for the hydratase active site and the dehydrogenase active site [13–15]. Schulz and coworkers have shown that for the substrate 2E,4E-decadienoyl-CoA efficient channeling of the intermediate between the two active sites is observed [16]. Substrate

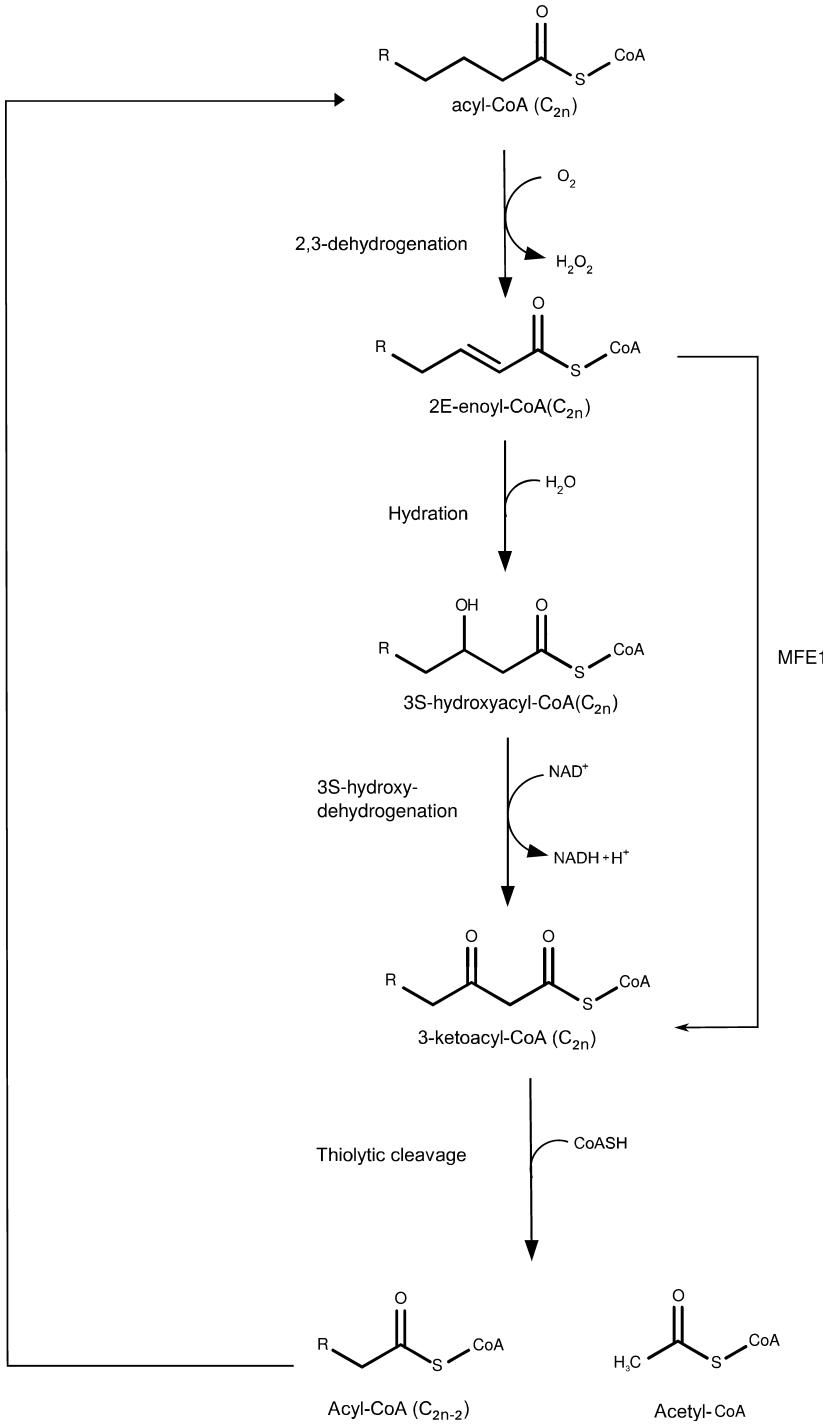

Fig. 1. The four reactions of the peroxisomal β-oxidation pathway. MFE1 catalyzes the second (hydration) and the third (3S-hydroxyacyl-CoA dehydrogenation) reaction.

channeling is an intriguing property of some enzyme systems [17], being well established for the mitochondrial β-oxidation pathway [18]. However, at the molecular level, the substrate channeling mechanism of such bulky and polar, substrate molecules is poorly understood [19].

The crystal structure of rat peroxisomal MFE1 (rpMFE1, 722 residues) (complexed with CoA) has been reported [20]. Five domains (A, B, C, D, and E) have been recognized in this fold (Fig. 2, Fig. S1). Its N-terminal part (catalyzing the hydratase reaction) has the crotonase fold (formed by the A and B domains), like the well-studied monofunctional Δ^2-enoyl-CoA hydratases [21]. The C-terminal part (catalyzing the dehydrogenase reaction) adopts the 3S-hydroxyacyl-CoA dehydrogenase (HAD) fold, like that described for the monofunctional human HAD (HsHAD) [22]. This HAD part has two lobes, a NAD-binding domain (the C domain) and a substrate binding region (the D/E domains) (Fig. 2). The D and E domains interact tightly with each other and have a very similar fold. The N-terminal and C-terminal parts of MFE1 are connected via a helical linker region. This linker region (domain B) functionally belongs to the crotonase fold, being the helix-10 of this fold, but structurally it belongs to the C-terminal HAD part (Fig. 2). The E domain has stabilizing interactions with this linker helix via hydrophobic interactions (by residues of EH2) and

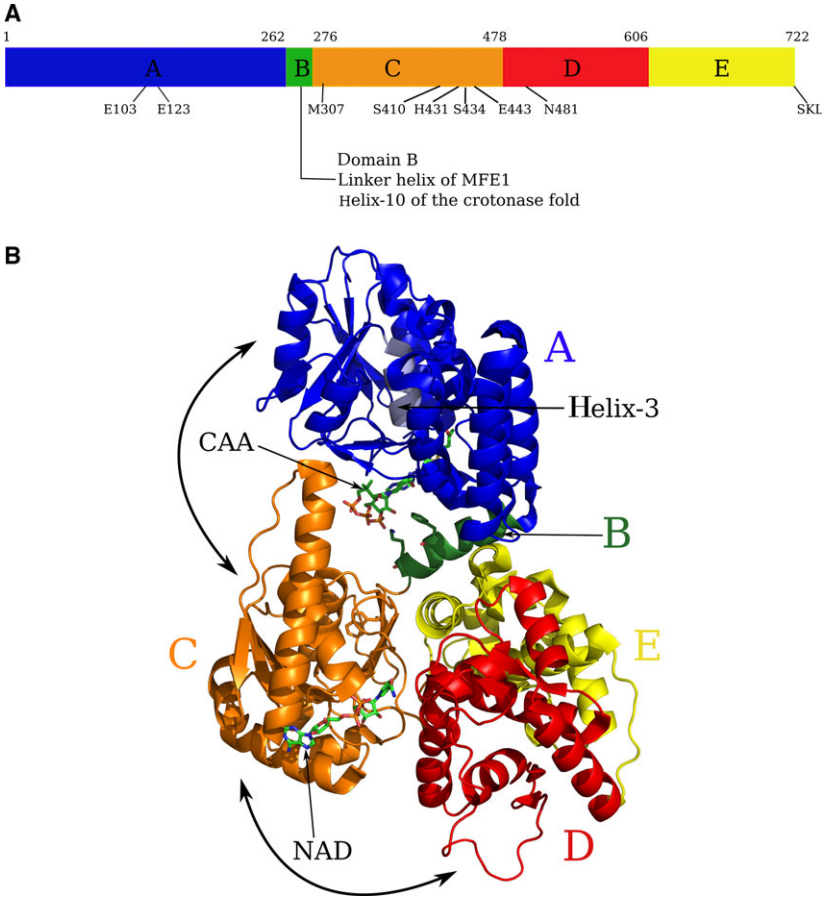

Fig. 2. The five MFE1 domains. (A) Schematic division of the MFE1 sequence in five domains. Domain B is also referred to as the linker helix or the helix-10. Glu103 and Glu123 are the catalytic residues of the A domain. Met307 contacts the nicotinamide moiety of NAD^+, and Ser410, His431, Ser434, Glu443, and Asn481 are important catalytic residues of the dehydrogenase domain. (B) The MFE1 fold, color-coded according to the domains (blue, domain A; green, domain B; orange, domain C; red, domain D; and yellow, domain E). Domains D and E have the same fold and are tightly interacting with each other. The ligands of this structure (5MGB) identify the hydratase active site (AcAc-CoA, labeled as CAA) and the dehydrogenase active site (NAD^+, labeled as NAD^+). The active site helix (the labeled 'helix-3' arrow points at its N terminus) of the hydratase domain, between Gly101 and Cys108, is colored light blue. The side chains of Phe271, Lys275, and Trp280 are shown as sticks. Phe271 and Lys275 of the linker helix (domain B) point toward the AcAc-CoA bound in the hydratase active site. Trp280 is at the C-terminal end of the linker helix. The bold arrows visualize the two hinge motions, being (a) of domain A with respect to the BCDE domains and (b) of domain C with respect to the D/E domains.

via a salt bridge (between Arg657 of the support loop (domain E) and Glu274 of the linker helix) [20]. The two active sites are about 40 Å apart, separated by a solvent-exposed tunnel. This tunnel is lined by an excess of positively charged residues [20], suggesting that substrate channeling of the negatively charged acyl-CoA molecules via electrostatic interactions with the positively charged tunnel surface could be important, as described for the thymidylate synthase–dihydrofolate reductase bifunctional enzyme [23,24].

The rpMFE1 Michaelis–Menten kinetic measurements reported here for short-chain substrates show that the catalytic efficiency of the two active sites of MFE1 is much lower than the efficiency of the corresponding monofunctional enzymes. The structural studies concern the analysis of the structure of rpMFE1 complexed with AcAc-CoA and NAD^+. In the available MFE1 crystal structures, there are two molecules in the asymmetric unit. In these two molecules, referred to as molecule A and molecule B, the domains adopt different conformations with respect to each other (Fig. 2). The comparison of these crystal structures suggests that this conformational flexibility of MFE1 is of key importance for the proper functioning of this enzyme.

Materials and methods

Expression and purification of rat peroxisomal MFE1

The cloning of the rpMFE1 (UniProt P07896) into pET15b vector has been described previously [20]. The expression and purification protocols of rpMFE1 were the same as reported previously [25]. At the end of the purification protocol, the concentrated protein was loaded on a Superdex-200 size exclusion chromatography column which was pre-equilibrated with gel filtration buffer (10 mM piperazine-N, N′-bis(2-ethanesulfonic acid (PIPES), 50 mM NaCl, pH 6.5). The peak fractions of the protein were pooled, concentrated, and stored at −70 °C.

Enzyme assays

The enzyme kinetic measurements were taken by following the reaction with the JASCO V660 spectrophotometer (JASCO Corporation, Tokyo, Japan) at 25 °C for 3 min in a 1-cm cuvette using 0.5 mL assay volumes. In each assay the reaction was initiated by adding the enzyme. The k_{cat} and K_m values were determined using the JASCO software SPECTRAMANAGER. The substrates 2E-butenoyl-CoA (for the forward hydratase and dehydrogenase reactions), AcAc-CoA (for the reverse dehydrogenase reaction), NAD^+, and NADH were purchased from Sigma (Sigma Aldrich, St Louis, MS, USA).

The 2E-enoyl-CoA hydratase activity was measured by monitoring the disappearance of the C-C double bond of 2E-butenoyl-CoA to form 3S-hydroxybutanoyl-CoA. The assay buffer contained 50 mM tris(hydroxymethyl)-aminomethane (Tris) (pH 9.0), 50 mM KCl, and 50 $\mu g \cdot mL^{-1}$ BSA. The progress of the reaction was monitored at 263 nm, with 95 $ng \cdot mL^{-1}$ present in the cuvette. For calculating the initial rates, an absorption coefficient of 6700 $M^{-1} \cdot cm^{-1}$ was used.

The forward dehydrogenase assay of rpMFE1 uses as substrate 2E-butenoyl-CoA, which is converted by the hydratase active site into 3S-hydroxybutanoyl-CoA. This then is the substrate of the dehydrogenase active site, which catalyzes the dehydrogenation of 3S-hydroxybutanoyl-CoA into acetoacetyl-CoA in the presence of NAD^+, being converted into NADH. The reaction mixture contained 50 mM Tris (pH 9), 50 mM KCl, 50 $\mu g \cdot mL^{-1}$ BSA, and 1 mM NAD^+. The reaction was carried out with 950 $ng \cdot mL^{-1}$ in the cuvette and the reaction was monitored at 340 nm (e_{340} = 6220 $M^{-1} \cdot cm^{-1}$).

The reverse dehydrogenase assay measures the conversion of the substrate AcAc-CoA into 3S-hydroxybutanoyl-CoA by the dehydrogenase active site of rpMFE1, using as assay buffer 50 mM Tris/HCl, 50 mM KCl, 50 $\mu g \cdot mL^{-1}$ BSA pH 7.0, and 0.1 mM NADH. The activity was monitored at 340 nm by following the disappearance of NADH with 950 $ng \cdot mL^{-1}$ present in the cuvette.

Crystallization, data collection, data processing, and structure refinement of the AcAc-CoA/NAD^+ complex

The AcAc-CoA/NAD^+ complex structure was obtained from a crystal grown at room temperature by cocrystallization in the presence of AcAc-CoA and NAD^+ using otherwise the same crystallization protocol as previously described for the CoA-complexed crystal form [25]. Briefly, these crystals were grown at room temperature using the sitting drop method. The protein solution was 8 $mg \cdot mL^{-1}$ in 10 mM PIPES, pH 6.5 and 50 mM NaCl, 2 mM AcAc-CoA, and 2 mM NAD^+, and the well solution was 100 mM 2-(N-morpholino) ethanesulfonic acid, pH 6.0, 150 mM ammonium sulfate, and 15% PEG4000 (w/v). Before data collection, the crystal was cryoprotected by a brief soak in well solution complemented with 15% glycerol, 2 mM AcAc-CoA, and 2 mM NAD^+. The data set of the AcAc-CoA/NAD^+ complex was collected at ESRF in Grenoble, France (Table 1). The data set was processed with iMOSFLM [26] and scaled using SCALA [27]. The statistics of the data processing are summarized in Table 1. The space group and cell dimensions are the same as previously found for the CoA-complexed crystal form [20] and there are two molecules per asymmetric unit. The initial phases were obtained by a rigid body refinement by REFMAC5 [28] using as a starting model the rpMFE1 model of the

Table 1. Data collection and refinement statistics.

Crystal form	The AcAc-CoA/NAD^+ complex crystal form, with bound AcAc-CoA and NAD^+
PDB entry code	5MGB
Beam line	ID14-2 (ESRF)
Temperature (K)	100
Wavelength (Å)	0.933
Space group	$P2_12_12_1$
Unit cell parameters (Å)	65.23 125.82 223.90
Number of molecules per asymmetric unit	2
V_m ($Å^3$/Da)	2.8
Resolution range (Å)[a]	35.0–2.8 (2.95–2.8)
Completeness (%)[a]	83.8 (84.2)
$<I/\sigma(I)>$[a]	8.0 (2.4)
R_{pim} (%)[a]	6.0 (23.0)
Number of unique reflections[a]	38 432 (5578)
Redundancy[a]	3.8 (3.1)
Wilson B factor ($Å^2$)	67
Refinement	
Resolution (Å)	33.6–2.8
R_{factor} (%)	20.9
R_{free} (%)	26.1
Total number of reflections	36 256
Number of protein atoms	11 092
Number of waters	96
Number of other molecules glycerol/sulfate	2/4
Rmsd, protein bonds (Å)	0.008
Rmsd, protein angles (°)	1.3
Rmsd B factor	
Protein main chain A, B ($Å^2$)	1.4, 1.4
Protein side chain A, B ($Å^2$)	1.5, 1.5
Average B factor	
Protein molecule, A/B ($Å^2$)	49/60
A-hydratase active site ligand (AcAc-CoA) ($Å^2$)	65
A-dehydrogenase active site ligand (NAD^+) ($Å^2$)	63
B-hydratase active site ligand (AcAc-CoA) ($Å^2$)	57
B-dehydrogenase active site ligand (NAD^+) ($Å^2$)	63
Ramachandran plot[b]	
Favored (%)	97.2
Allowed (%)	2.8
Outliers (%)	0

[a] The numbers in parentheses refer to the outer shell. [b] Calculated using Rampage [45].

CoA-complexed structure (2X58), in which the solvent and ligand molecules were removed. The structure was refined further with REFMAC5 at 2.8 Å resolution, using NCS restraints. The active site ligands were modeled in the maps using COOT [29] at the end of the refinement. The structure was validated and improved using MolProbity [30] and COOT. The refinement was stopped once the remaining peaks in the electron density maps, at approximately 5 sigma, did not have structural information. The final refinement statistics are summarized in Table 1.

Structure analysis

In the AcAc-CoA/NAD^+ complex, structure molecules A and B have been built completely from residues −4 to 720 and from residues −1 to 718, respectively. The most flexible regions, having high B factors in both molecules, are loop-2 of the hydratase domain (near residue 70), the tip of the CH2 helix of the C domain (near residue 355), the substrate specificity loop of domain D (near residue 545), the β-meander of the D domain (near residue 587), and the loop between domains D and E (near residue 610). The structure of molecule A has been used for the structure analysis, employing programs of the CCP4 package [31], unless stated otherwise.

The rpMFE1 hydratase active site (liganded with AcAc-CoA) has been compared with the liganded monofunctional hydratase active site (liganded with AcAc-CoA (1DUB) [32]) as well as with the rpMFE1 active site (complexed with CoA (2X58) [20], with 3S-hydroxydecanoyl-CoA (3ZWC) [25] and unliganded (3ZW8) [25]) by superimposing the rpMFE1 hydratase domain and the hydratase subunit on each other, using the SSM superpositioning option of COOT [33].

For the characterization of the open/closed conformations of the HAD part of rpMFE1, several crystal structures of HsHAD have been used, in particular the ternary complexed, fully closed structure (1F0Y) [22] and the binary complexed structures with NAD^+ (3HAD) [34] and NADH (1F17) [22]. For these comparisons, two superposition protocols (employing the SSM superpositioning option of COOT) were used, being either (a) superimposing the C domain of rpMFE1 on the NAD-binding domain of HsHAD or (b) superimposing the D/E domains of rpMFE1 on the two assembled dimerization domains of the HsHAD dimer.

Results and discussions

The rpMFE1 enzyme kinetic studies with the short-chain 2E-butenoyl-CoA and AcAc-CoA substrates

The enzyme kinetic data for short-chain substrates (having a four-carbon atom acyl chain) are summarized in Table 2. These kinetic data have been measured with 2E-butenoyl-CoA (also known as crotonyl-CoA, in the forward direction) and AcAc-CoA (in the reverse direction) as the substrates. The forward hydratase and the forward NAD^+ dependent dehydrogenase reaction rates are at least 10-fold lower than the rates for the corresponding monofunctional

Table 2. The Michaelis–Menten kinetic constants of the hydratase and the dehydrogenase activities of MFE1 and of the corresponding monofunctional enzymes

Enzyme, assay	Substrate	k_{cat} (s^{-1})	K_m (μM)	k_{cat}/K_m ($M^{-1}·s^{-1}$)	Comments	References
rpMFE1 (short-chain substrates)						
Hydratase	2E-Butenoyl-CoA	113.0 ± 33.0	82.0 ± 18.0	1.4*10^6	pH 9.0	This work
Dehydrogenase, forward	3S-Hydroxybutanoyl-CoA	1.7 ± 0.1	3.6 ± 1.0	0.5*10^6	pH 9.0	This work
Dehydrogenase, reverse	AcAc-CoA	23.0 ± 2.3	44.0 ± 15.0	0.5*10^6	pH 7.0	This work
rpMFE1 (medium-chain substrates)						
Hydratase	2E-Hexenoyl-CoA	102	9	11*10^6	pH 8.0, linked assay: HAD	[38]
Hydratase	2E-Decenoyl-CoA	80	21	3.8*10^6	pH 8.0, linked assay: HAD	[38]
Hydratase	2E,4E-Decadienoyl-CoA	1.7	24	0.07*10^6	pH 8.0, linked assay: HAD and thiolase	[16]
Dehydrogenase, forward	3S-Hydroxyhexanoyl-CoA	22	11	2.0*10^6	pH 10.2, linked assay: hydratase	[7]
Monofunctional enzymes (short-chain substrates)						
Bovine hydratase	2E-Butenoyl-CoA	1000	40	25.0*10^6	pH 7.5	[37,46]
Bovine HAD, forward	3S-Hydroxybutanoyl-CoA	200	75	2.7*10^6	pH 10.0	[36]
HsHAD, reverse	AcAc-CoA	250	15	16.7*10^6	pH 7.0	[35]

enzymes [35–37]. The k_{cat} for the hydratase reaction (113 s^{-1}) is much higher than the k_{cat} for the forward dehydrogenase reaction (1.7 s^{-1}), as previously observed also for substrates with longer acyl chains (Table 2), whereas the K_m values for the hydratase and forward dehydrogenase reactions are 82 and 3.6 μM, respectively. The k_{cat} and K_m values for the reverse dehydrogenase reaction, using AcAc-CoA as substrate, are, respectively, 23 s^{-1} and 44 μM, having therefore a k_{cat} that is also about 10-fold lower than of the monofunctional enzyme. In the forward dehydrogenase assay of MFE1, the substrate is generated by its hydratase active site, which therefore functions as a linker enzyme, generating the dehydrogenase substrate. As the hydratase k_{cat} is much higher than the forward dehydrogenase k_{cat} for the short-chain substrate, it can be assumed that in this assay (Table 2) the hydratase reaction is not the rate-limiting step, being independent from possible substrate channeling. Substrate channeling of MFE1 has been reported in case the substrate is 2E,4E-decadienoyl-CoA, for which the k_{cat} and K_m values of the hydratase reaction were determined to be 1.7 s^{-1} and 24 μM, respectively [16] (Table 2), whereas for the 2E-decenoyl-CoA substrate the k_{cat} and K_m values of the hydratase reaction were determined to be 80 s^{-1} and 21 μM, respectively [38] (Table 2).

The structure of the hydratase active site of rpMFE1 complexed with AcAc-CoA

In the AcAc-CoA/NAD^+ complex structure, refined at 2.8 Å resolution (Table 1), the AcAc-CoA is only bound in the hydratase active site. Its mode of binding is well defined by the electron density map (Fig. S2), adopting its characteristic bent conformation. The thioester oxygen of AcAc-CoA is hydrogen bonded to the peptide NH-groups of Ala61 (loop-2, Fig. S1) and Gly100 (N terminus of the helix-3) (Fig. 3A). The 3-keto oxygen is hydrogen bonded to the carboxylate oxygens of Glu103 and Glu123, like in the complex of the monofunctional hydratase [32], suggesting that the carboxylate moieties of both catalytic glutamates are protonated in this complex. The acetoacetyl moiety is bound in a somewhat twisted conformation (Fig. 3A), whereas it is bound in a planar conformation in the active site of the monofunctional hydratase [32]. The twisted conformation of the acetoacetate moiety is not possible in the monofunctional hydratase active site, due to the presence of the more bulky side chain of Trp120 in this active site, which is Leu75 (helix-2) in MFE1 (Fig. S3). In molecule B, the side chain of Leu73 (of the flexible loop-2) is also pointing into the active site, but in molecule A, due to conformational differences in loop-2, correlated with different crystal packing, the Leu73 side chain is pointing outward. In the crotonase fold enzymes, the active site is covered by the C-terminal helix, helix-10, which in MFE1 functions also as the linker helix, domain B (Fig. 2). Sequence conservation suggests that a basic residue of helix-10 is important for its function, forming a salt bridge with a phosphate group of the substrate. Also, a hydrophobic residue pointing to the pantetheine moiety of CoA is conserved [39,40] in the crotonase fold. In the MFE1 helix-10, the basic residue, Lys275, forms a salt bridge with the pyrophosphate group of

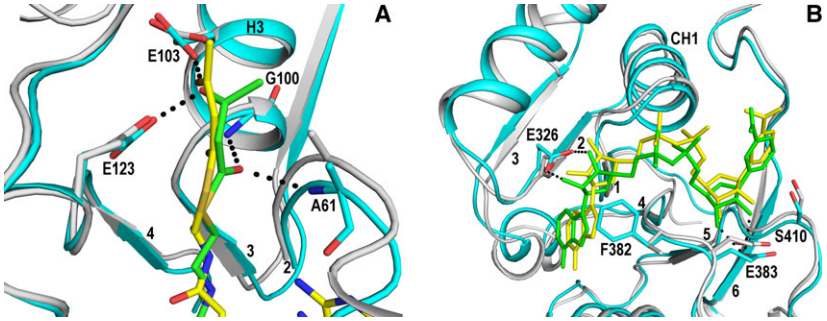

Fig. 3. Comparison of the structures of the liganded active sites of MFE1 and its monofunctional counterparts. (A) The hydratase active site. Comparison of the mode of binding of AcAc-CoA to the hydratase active site of MFE1 (cyan, 5MGB) and to the active site of the monofunctional hydratase (gray, 1DUB). The MFE1 residues are labeled. The oxyanion hole of MFE1 is formed by N(Ala61) (loop-2) and N (Gly100) (helix-3). The catalytic residues are Glu103 and Glu123. H3 identifies the active site helix (helix-3) and the numbers 2, 3, and 4 identify loop-2 and β-strands B3 and B4 of domain A, respectively. Dotted lines (black) mark the hydrogen bonds of the thioester and the 3-keto oxygen atoms with the oxyanion hole peptide NH-groups and the catalytic glutamates, respectively. (B) The mode of binding of NAD^+ in the structures of binary complexes. For this comparison, domain C of MFE1 (cyan, 5MGB) has been superimposed on the NAD-binding domain of HsHAD (gray, 3HAD). CH1 identifies the helix that interacts with the NAD pyrophosphate moiety and the numbers 1 to 6 identify the β-strands CB1 to CB6 of the Rossmann fold of domain C. Glu326 interacts with the ribose moiety of the ADP part of NAD^+. The side chain of Phe382 contacts also the ADP-ribose moiety. Glu383 is hydrogen bonded to the nicotinamide-ribose moiety and to the main chain of the loop after CB5, identified by the labeled Ser410 (which corresponds to Ser137 of HsHAD). Dotted lines (black) mark the hydrogen bond interactions of the Glu326 and Glu383 side chains, respectively, with the ADP-ribose and the nicotinamide-ribose moieties of NAD^+.

the CoA moiety and the hydrophobic residue, pointing to the pantetheine moiety, is Phe271. Phe271 is part of a conserved hydrophobic cluster that includes Ile63 and Leu126 (Fig. S3). Ile63 and Leu126 protrude out of loop-2 and loop-4, respectively, anchoring helix-10 to domain A of the crotonase fold.

The structure of the HAD active site of rpMFE1 complexed with NAD^+

NAD^+ is bound to the C domain, in a deep cleft between the C domain and the D/E domains (Fig. 2, Fig. S4). The mode of binding of NAD^+ to the HAD active site is well defined by the respective electron density map (Fig. S2), except for the nicotinamide moiety whose atoms have relatively high B factors, like in HsHAD [22]. The NAD^+ mode of binding to MFE1 is the same as for NADH, which is also well defined by its electron density, including its nicotinamide moiety (Fig. S2) [25] and which interacts with the side chain of the conserved Met307 (Fig. S5). The affinity of MFE1 for NADH (K_d = 1 μM) is much higher than for NAD^+ (K_d = 120 μM) [7], like also reported for HsHAD [34]. The mode of binding of NAD^+ to MFE1 is also very similar as seen in HsHAD (Fig. 3B, Fig. S5). The dimeric HsHAD, consisting of two identical subunits, has a broad substrate specificity, such that the length of the acyl chain of its substrate, 3S-hydroxyacyl-CoA, extends from 4 to 16 carbons [36]. Each subunit adopts a bilobal fold. The sequence alignment of HsHAD and rpMFE1 is given in Fig. S1. The sequence identity between the HAD part of rpMFE1 and HsHAD is 31%. Compared to MFE1, HAD is missing the A, B, and E domains of MFE1 (Fig. S1). The N-terminal, NAD-binding domain of HsHAD corresponds to the MFE1 C

Fig. 4. The open and closed conformations of domain C with respect to the D/E domains. Domain C of MFE1 corresponds to the NAD-binding domain of HsHAD. The D/E domains of MFE1 correspond to the two assembled dimerization domains of HsHAD. The latter MFE1 and HsHAD units have been superimposed on each other in each of the panels. The view is toward the active site along the dimer twofold axis of HsHAD. The visualized MFE1 Cα-trace includes the B, C, D, and E domains. W280 identifies Trp280 at the C-terminal end of domain B. The HsHAD Cα-trace covers the complete dimer. Residues of the Cβ6-Cβ7 loop (of the NAD-binding domain in HsHAD, domain C in MFE1), and of the two DH2-DH3 loops (of the dimerization domains in HsHAD, domains D/E in MFE1) shape the pantetheine binding tunnel (P-tunnel) of HsHAD and are highlighted in yellow. (A) Comparison of the unliganded, open structure of HsHAD (gray, 1F14) and liganded, closed structure of HsHAD (orange, 1F0Y, including the AcAc-CoA ligand and NAD^+). (B) Comparison of molecule B of MFE1 (cyan, 5MGB, fully open) and molecule A of MFE1 (green, 5MGB, partially closed). (C) Comparison of molecule B of MFE1 (cyan, 5MGB, fully open) and the unliganded, open conformation of HsHAD (gray, 1F14). (D) Comparison of molecule A of MFE1 (green, 5MGB, partially closed) with the liganded fully closed conformation of HsHAD (orange, 1F0Y, including the AcAc-CoA ligand and NAD^+).

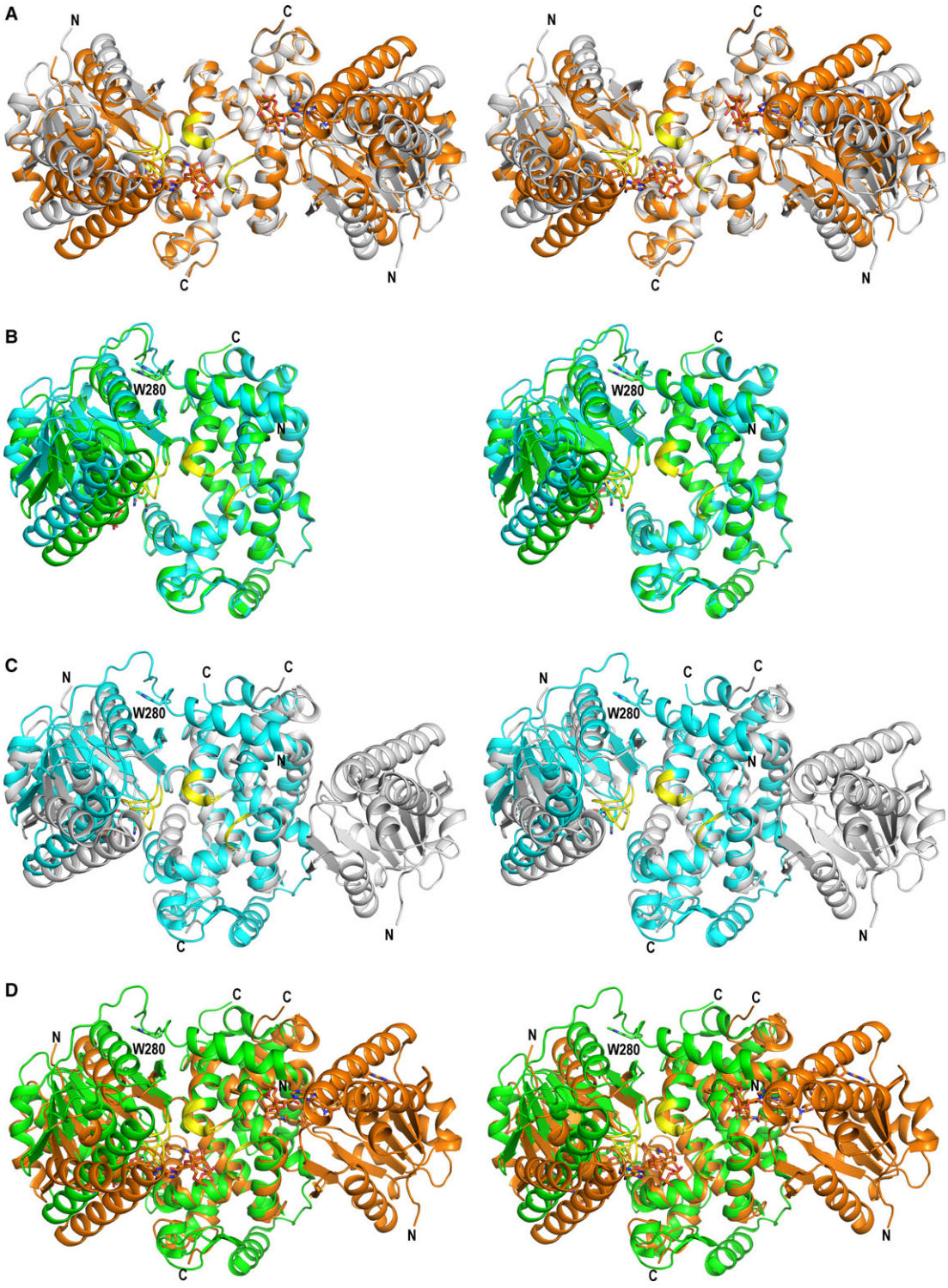
A
N
C
C
N
N
C
C
N
B
W280
C
N
W280
C
N
C
W280
C
N
W280
C
N
C
C
C
N
C
N
C
C
N
W280
C
N
W280
C
N
D
W280
C
C
N
N
C
N
W280
C
C
N
N
C
N

domain and the two C-terminal dimerization domains of the HsHAD dimer correspond to the MFE1 D and E domains, respectively (Fig. 4). Structural studies of HsHAD have provided the crystal structures of HsHAD complexed with NAD^+, NADH, substrate (3S-hydroxybutanoyl-CoA), and a dead-end ternary complex with bound NAD^+ and AcAc-CoA [22]. In the latter complex, the N-terminal domain has moved toward the dimerization domain, such that HsHAD has adopted its fully closed conformation (Fig. 4), required for being able to catalyze its reaction. In this ternary complex, the pantetheine part of AcAc-CoA is bound in an extended tunnel (P-tunnel) between the CB6-CB7 loop of the NAD-binding domain, and the two DH2-DH3 loops of the HsHAD dimerization domains (Fig. 4).

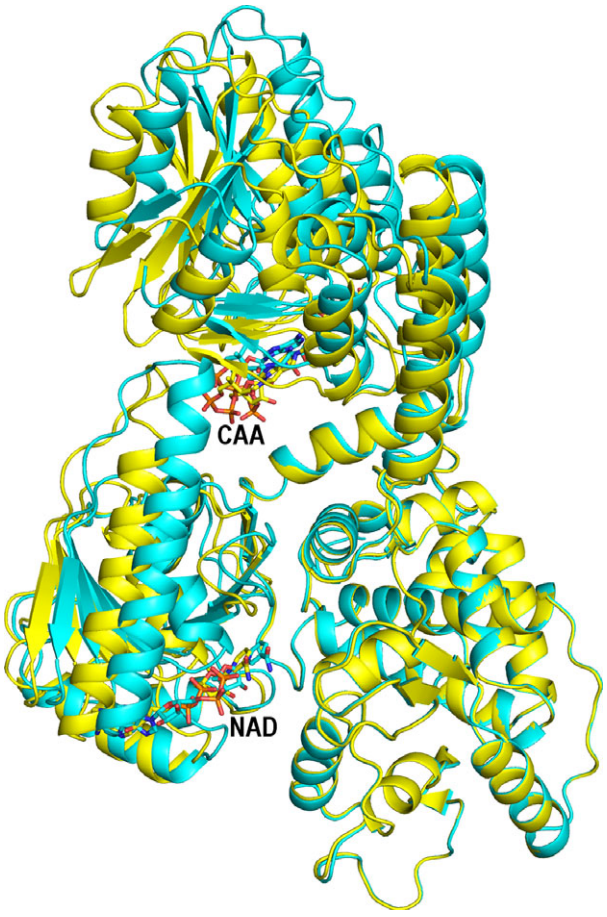

Fig. 5. The conformational flexibility of MFE1. Comparison of molecule A (cyan) and molecule B (yellow), such that the D/E domains of both molecules (5MGB) have been superimposed. The bound AcAc-CoA (labeled CAA, domain A, upper part) and NAD^+ (labeled NAD, bound to domain C, in the groove between domain C and the D/E domains, lower part) are presented as sticks using atom-type coloring.

In the AcAc-CoA/NAD^+ complex structure of MFE1, NAD^+ only interacts with the C domain (Fig. S5) and no domain closure is induced by its binding. The pyrophosphate moiety binds at the N terminus of helix CH1 of the N-terminal βαβ-unit (CB1-CH1-CB2, Fig. 3B) of the Rossmann fold of the C domain. As is observed in other NAD-binding βαβ-units [41,42], a glutamate at the end of the second β-strand (CB2, Glu326) interacts with the ribose moiety of the adenosine part. The side chain of Phe382, at the end of the CB4 β-strand, swings from a solvent-exposed conformation in the absence of bound NAD toward covering the ADP-ribose moiety in the presence of NAD^+ as well as NADH (Fig. 3B, Fig. S4). No other conformational changes are induced on binding NAD^+ or NADH. A second glutamate (Glu383, also at the end of CB4) interacts with the hydroxyl groups of the nicotinamide-ribose group. The Glu383 side chain (corresponding to Glu110 in HsHAD) is also anchored to N (Ser410) and N(Ala411) of the loop after CB5 (Fig. S5). These hydrogen bond interactions have also been described for the structures of the HsHAD binary complexes. Ser410 corresponds to Ser137 in HsHAD, and in HsHAD, this 'Ser137-loop' adopts a different conformation in its ternary complex [22].

The conformational flexibility of MFE1

In the crystal form of MFE1 used here for its structural characterization, the conformations of the HAD part of molecules A and B are different (Fig. 5). These conformational differences are related to differences in crystal packing and these conformational differences are seen in each of the available rpMFE1 crystal structures (Table 3). In molecule A, the HAD part adopts a partially closed conformation, whereas in molecule B it is fully open, because of a rotation of domain C, away from the D/E domains (Video S1). This is a rigid body rotation. Superpositioning of domain C of molecules A and B results in an rmsd for corresponding Cα atoms of 0.2 Å (excluding only the tip of the flexible CH2-helix). The conformational differences in the HAD part can be quantified by measuring the distance between Cα(Thr306) (N-terminal CH1 helix) and Cα (Ala524) (C-terminal DH3 helix) (Fig. S4, Table 3). These two residues are located on the opposite sides of the cleft that binds the NAD cofactor. Helices CH1 and DH3 point away from the cleft (Fig. S4). The distances between the residues at the C terminus and N terminus of helices CH1 and DH3, respectively, of molecules A and B are also listed (Table 3). The residues in HsHAD corresponding to Thr306 and Ala524 are Leu25 and Val253, respectively (Fig. S1). The

Table 3. Conformational differences between the active sites of molecule A and molecule B[a]

Crystal form	The AcAc-CoA/NAD^+ complex crystal form, with bound AcAc-CoA and NAD^+ (this paper)	The 3S-hydroxydecanoyl-CoA complex crystal form, with bound 3S-hydroxydecanoyl-CoA and NADH [25]	The unliganded crystal form [25]	The CoA complex crystal form with bound CoA [20]
Experimental conditions	Cocrystallization experiment with AcAc-CoA and NAD^+	Crystal first grown as the CoA complex. Subsequently obtained after the washing steps, followed by a soaking experiment with 2E-decenoyl-CoA and NADH	Crystal first grown as the CoA complex. Subsequently obtained after washing steps, by which CoA is removed	Crystal grown by cocrystallization in the presence of CoA
PDB entry code	5MGB	3ZWC	3ZW8	2X58
Hydratase active site (molecule A)				
Active site ligand	AcAc-CoA	3S-Hydroxydecanoyl-CoA	Sulfate	CoA
Gly100-Phe271[b]	17.3	17.6	17.5	17.9
Cys108-Trp280[b]	42.0	42.4	42.2	42.8
Dehydrogenase active site (molecule A)				
Active site ligand	NAD^+	NADH	Water	ADP
Thr306-Ala524[c]	10.2	10.2	10.9	11.1
Ala316-Phe518[c]	33.1	33.0	33.1	33.3
Hydratase active site (molecule B)				
Active site ligand	AcAc-CoA	3S-Hydroxydecanoyl-CoA	Sulfate	CoA
Gly100-Phe271[b]	16.6	16.9	17.1	16.9
Cys108-Trp280[b]	40.4	40.7	40.7	40.7
Dehydrogenase active site (molecule B)				
Active site ligand	NAD^+	NADH	Sulfate	Sulfate
Thr306-Ala524[c]	12.8	12.9	13.6	13.5
Ala316-Phe518[c]	34.9	34.9	34.9	34.9

[a] The crystal packing in each of these structures is the same.

[b] The listed distance (in Å) is between the Cα atoms of the given residues. These residues are also identified in Fig. 2.

[c] The listed distance (in Å) is between the Cα atoms of the given residues. These residues are also identified in Fig. S4.

It can be noted that for each of the four structures, the HAD active site of molecule A is more closed than in molecule B, whereas its hydratase active site is more open.

distance between these Cα atoms is 8.3 Å in the fully closed HsHAD active site and 12.0 Å for the fully open HsHAD active site. For the MFE1 active site, this distance is 10.2 Å for the molecule A of the AcAc-CoA/NAD^+ complex and it is 12.8 Å for its molecule B (Table 3). In the HsHAD ternary complex, the NAD-binding domain has moved further toward the dimerization domain than in molecule A of the MFE1 complex, adopting a fully closed conformation with tight stacking interactions between the nicotinamide group and the 3-keto group [22]. The hinge region of this motion appears to be the regions 201–207 in HsHAD [35] and 474–480 in rpMFE1 (Fig. 4).

This rigid body motion toward a more closed conformation of domain C is correlated with an upward movement of domain A, adopting a more open conformation, away from the HAD part (Fig. 5, Video S1) in molecule A. The domain A movement is also a rigid body motion. Superpositioning of domain A of molecules A and B results in an rmsd for corresponding Cα atoms of 0.3 Å (excluding only the flexible loop-2 region). The conformational difference is also seen from the distance information provided in Table 3. The distance between Cα(Gly100) and Cα (Phe271) is 17.3 Å in molecule A, and it is 0.7 Å shorter in molecule B. This distance measures the distance between the N terminus of the active site helix-3 and the middle part of the linker helix, Phe271, whose side chain contacts the bound substrate (Fig. 2). The hinge region is near the N terminus of domain B (Video S1, Fig. 5). In this conformational movement, domain A of molecule A moves away from the linker helix and a comparison of distances between atoms further away from the hinge region (between Cα (Cys108), at the end of helix-3, and Cα(Trp280), at the end of the linker helix) show larger differences, from 42.0 Å in molecule A to 40.4 Å in molecule B.

Clearly, MFE1 has two hinge motions, being the movement of the A domain with respect to the BCDE part (more open in molecule A) and the open/closed conformational switch of the HAD part (more closed in molecule A), being the movement of the C domain with respect to the D/E domains. The structure comparisons with HsHAD (Fig. 4) suggest that the HAD part of

molecule A is only partially closed in this crystal form. In this partially closed form, domain A moves away from domain B (Table 3). Domain B is an integral part of the crotonase fold, being helix-10. Experimental studies have addressed the importance of domain B (helix-10) for full MFE1 activity. The interactions of the B domain (helix-10) with the D/E domains are important for full hydratase activity of MFE1, which was shown by extensive MFE1 deletion experiments, as it was found that a deletion mutant in which the C domain was deleted still has full hydratase activity [38], whereas constructs without the D/E part have lost the hydratase activity. Additionally, point mutation studies of helix-10 of a model enzyme of the crotonase superfamily fold have shown the critical importance of helix-10 for the catalytic properties of this model enzyme. In this model enzyme, Δ^3,Δ^2-enoyl-CoA isomerase, the residue that corresponds to Phe271 (Fig. 2) in MFE1, was mutated into an alanine, and this point mutation variant was much less active than wild-type [39,40]. Further rotation of the C domain of MFE1 toward a fully closed HAD structure will likely move the A domain further from its HAD BCDE part and from its helix-10 (domain B), and therefore this will affect the interactions between domain A and its helix-10, being an integral part of the HAD part of MFE1. These structural changes are therefore expected to affect the binding and catalytic properties of the hydratase active site of MFE1. Therefore, the correlated motions of the HAD part and the A domain could function as an allosteric control mechanism [43,44] between the dehydrogenase and hydratase active sites, facilitating substrate channeling of tightly bound intermediates by inducing the release of the product of the hydratase active site when the dehydrogenase active site is complexed with NAD^+. In this respect, it is interesting that for HsHAD the binding of NAD^+ precedes the binding of substrate and the affinity for its substrate is much increased after binding of NAD^+ [22].

Concluding remarks

In MFE1, the hydratase and dehydrogenase active sites are built by one polypeptide chain. The conformational flexibility of these two parts with respect to each other provides additional complexity to the catalytic properties of MFE1, as compared to the corresponding monofunctional homologues. This additional complexity correlates with lower catalytic rates of MFE1 for short-chain substrates, being 10-fold (or more) lower than of these counterparts. The presence of open and closed conformations of the HAD part of MFE1 is in common with the monofunctional HAD. However, in this MFE1 crystal structure, obtained by cocrystallization in the presence of AcAc-CoA and NAD^+, the fully closed, ternary complex conformation, as seen in HsHAD, is not captured. AcAc-CoA is only bound in the hydratase active site and not in the HAD active site. Further structural studies of rpMFE1 aimed at capturing the fully closed conformation of its HAD part have been initiated.

Acknowledgements

The expert support from the staff of the ESRF beam line ID14-2 has been much appreciated. The use of the facilities and expertise of the Biocenter Oulu core facility, a member of Biocenter Finland and Instruct-FI, is gratefully acknowledged. The support of a Biocenter Finland Grant to RKW is gratefully acknowledged. The expert help of Ville Ratas has been very valuable.

Author contributions

PK and RKW planned the experiments; PK purified the protein and performed the crystallography experiments; PK, GBM, and SS performed the enzyme kinetic experiments; WS prepared reagents; PK, TRK, and RKW analyzed the structures and prepared the figures. RW, PK, TRK, and JKH wrote the manuscript.

References

1 Hiltunen JK, Filppula SA, Koivuranta KT, Siivari K, Qin YM and Hayrinen HM (1996) Peroxisomal beta-oxidation and polyunsaturated fatty acids. *Ann N Y Acad Sci* **804**, 116–128.
2 Wanders RJ (2014) Metabolic functions of peroxisomes in health and disease. *Biochimie* **98**, 36–44.
3 Poirier Y, Antonenkov VD, Glumoff T and Hiltunen JK (2006) Peroxisomal beta-oxidation – a metabolic pathway with multiple functions. *Biochim Biophys Acta* **1763**, 1413–1426.
4 van Weeghel M, te Brinke H, van Lenthe H, Kulik W, Minkler PE, Stoll MS, Sass JO, Janssen U, Stoffel W, Schwab KO *et al.* (2012) Functional redundancy of mitochondrial enoyl-CoA isomerases in the oxidation of unsaturated fatty acids. *FASEB J* **26**, 4316–4326.
5 Eaton S, Bursby T, Middleton B, Pourfarzam M, Mills K, Johnson AW and Bartlett K (2000) The mitochondrial trifunctional protein: centre of a beta-oxidation metabolon? *Biochem Soc Trans* **28**, 177–182.
6 Houten SM and Wanders RJ (2010) A general introduction to the biochemistry of mitochondrial fatty acid beta-oxidation. *J Inherit Metab Dis* **33**, 469–477.
7 Osumi T and Hashimoto T (1980) Purification and properties of mitochondrial and peroxisomal 3-

hydroxyacyl-CoA dehydrogenase from rat liver. *Arch Biochem Biophys* **203**, 372–383.
8 Palosaari PM and Hiltunen JK (1990) Peroxisomal bifunctional protein from rat liver is a trifunctional enzyme possessing 2-enoyl-CoA hydratase, 3-hydroxyacyl-CoA dehydrogenase, and Δ3, Δ2-enoyl-CoA isomerase activities. *J Biol Chem* **265**, 2446–2449.
9 Zhang D, Yu W, Geisbrecht BV, Gould SJ, Sprecher H and Schulz H (2002) Functional characterization of Δ3, Δ2-enoyl-CoA isomerases from rat liver. *J Biol Chem* **277**, 9127–9132.
10 Hashimoto T (1999) Peroxisomal beta-oxidation enzymes. *Neurochem Res* **24**, 551–563.
11 Houten SM, Denis S, Argmann CA, Jia Y, Ferdinandusse S, Reddy JK and Wanders RJ (2012) Peroxisomal L-bifunctional enzyme (Ehhadh) is essential for the production of medium-chain dicarboxylic acids. *J Lipid Res* **53**, 1296–1303.
12 Ding J, Loizides-Mangold U, Rando G, Zoete V, Michielin O, Reddy JK, Wahli W, Riezman H and Thorens B (2013) The peroxisomal enzyme L-PBE is required to prevent the dietary toxicity of medium-chain fatty acids. *Cell Rep* **5**, 248–258.
13 Xu R and Cuebas DA (1996) The reactions catalyzed by the inducible bifunctional enzyme of rat liver peroxisomes cannot lead to the formation of bile acids. *Biochem Biophys Res Commun* **221**, 271–278.
14 Kurosawa T, Sato M, Inoue K, Yoshimura T, Thoma M, Jiang LL and Hashimoto T (1998) Separation of stereoisomers of C27-bile acid CoA esters by liquid chromatography and its application to the study of the stereospecificities of D- and L-bifunctional proteins in bile acids biosynthesis. *Anal Chim Acta* **365**, 249–257.
15 Kurosawa T, Sato M, Nakano H, Fujiwara M, Murai T, Yoshimura T and Hashimoto T (2001) Conjugation reactions catalyzed by bifunctional proteins related to beta-oxidation in bile acid biosynthesis. *Steroids* **66**, 107–114.
16 Yang SY, Cuebas D and Schulz H (1986) Channeling of 3-hydroxy-4-trans-decenoyl coenzyme A on the bifunctional beta-oxidation enzyme from rat liver peroxisomes and on the large subunit of the fatty acid oxidation complex from *Escherichia coli*. *J Biol Chem* **261**, 15390–15395.
17 Srere PA (2000) Macromolecular interactions: tracing the roots. *Trends Biochem Sci* **25**, 150–153.
18 Nada MA, Rhead WJ, Sprecher H, Schulz H and Roe CR (1995) Evidence for intermediate channeling in mitochondrial beta-oxidation. *J Biol Chem* **270**, 530–535.
19 Wheeldon I, Minteer SD, Banta S, Barton SC, Atanassov P and Sigman M (2016) Substrate channelling as an approach to cascade reactions. *Nat Chem* **8**, 299–309.
20 Kasaragod P, Venkatesan R, Kiema TR, Hiltunen JK and Wierenga RK (2010) Crystal structure of liganded rat peroxisomal multifunctional enzyme type 1: a flexible molecule with two interconnected active sites. *J Biol Chem* **285**, 24089–24098.
21 Zhang H, Machutta CA and Tonge PJ. (2010) Fatty acid biosynthesis and oxidation. In *Comprehensive Natural Products Chemistry II Chemistry and Biology* (Mander L and Lui H-W, Eds), vol. **8**, pp. 231–275. Elsevier, Oxford.
22 Barycki JJ, O'Brien LK, Strauss AW and Banaszak LJ (2000) Sequestration of the active site by interdomain shifting. Crystallographic and spectroscopic evidence for distinct conformations of L-3-hydroxyacyl-CoA dehydrogenase. *J Biol Chem* **275**, 27186–27196.
23 Sharma H, Landau MJ, Vargo MA, Spasov KA and Anderson KS (2013) First three-dimensional structure of *Toxoplasma gondii* thymidylate synthase-dihydrofolate reductase: insights for catalysis, interdomain interactions, and substrate channeling. *Biochemistry* **52**, 7305–7317.
24 Anderson KS (2017) Understanding the molecular mechanism of substrate channeling and domain communication in protozoal bifunctional TS-DHFR. *Protein Eng Des Sel* **30**, 253–261.
25 Kasaragod P, Schmitz W, Hiltunen JK and Wierenga RK (2013) The isomerase and hydratase reaction mechanism of the crotonase active site of the multifunctional enzyme (type-1), as deduced from structures of complexes with 3S-hydroxy-acyl-CoA. *FEBS J* **280**, 3160–3175.
26 Powell HR, Johnson O and Leslie AG (2013) Autoindexing diffraction images with iMosflm. *Acta Crystallogr D Biol Crystallogr* **69**, 1195–1203.
27 Evans P (2006) Scaling and assessment of data quality. *Acta Crystallogr D Biol Crystallogr* **62**, 72–82.
28 Murshudov GN, Skubak P, Lebedev AA, Pannu NS, Steiner RA, Nicholls RA, Winn MD, Long F and Vagin AA (2011) REFMAC5 for the refinement of macromolecular crystal structures. *Acta Crystallogr D Biol Crystallogr* **67**, 355–367.
29 Emsley P and Cowtan K (2004) Coot: model-building tools for molecular graphics. *Acta Crystallogr D Biol Crystallogr* **60**, 2126–2132.
30 Chen VB, Arendall WB 3rd, Headd JJ, Keedy DA, Immormino RM, Kapral GJ, Murray LW, Richardson JS and Richardson DC (2010) MolProbity: all-atom structure validation for macromolecular crystallography. *Acta Crystallogr D Biol Crystallogr* **66**, 12–21.
31 Collaborative Computational Project, Number 4 (1994) The CCP4 suite: programs for protein crystallography. *Acta Crystallogr D Biol Crystallogr* **50**, 760–763.

32 Engel CK, Mathieu M, Zeelen JP, Hiltunen JK and Wierenga RK (1996) Crystal structure of enoyl-coenzyme A (CoA) hydratase at 2.5 angstroms resolution: a spiral fold defines the CoA-binding pocket. *EMBO J* **15**, 5135–5145.
33 Krissinel E and Henrick K (2004) Secondary-structure matching (SSM), a new tool for fast protein structure alignment in three dimensions. *Acta Crystallogr D Biol Crystallogr* **60**, 2256–2268.
34 Barycki JJ, O'Brien LK, Bratt JM, Zhang R, Sanishvili R, Strauss AW and Banaszak LJ (1999) Biochemical characterization and crystal structure determination of human heart short chain L-3-hydroxyacyl-CoA dehydrogenase provide insights into catalytic mechanism. *Biochemistry* **38**, 5786–5798.
35 Barycki JJ, O'Brien LK, Strauss AW and Banaszak LJ (2001) Glutamate 170 of human l-3-hydroxyacyl-CoA dehydrogenase is required for proper orientation of the catalytic histidine and structural integrity of the enzyme. *J Biol Chem* **276**, 36718–36726.
36 Kobayashi A, Jiang LL and Hashimoto T (1996) Two mitochondrial 3-hydroxyacyl-CoA dehydrogenases in bovine liver. *J Biochem* **119**, 775–782.
37 Xiang H, Luo L, Taylor KL and Dunaway-Mariano D (1999) Interchange of catalytic activity within the 2-enoyl-coenzyme A hydratase/isomerase superfamily based on a common active site template. *Biochemistry* **38**, 7638–7652.
38 Kiema TR, Taskinen JP, Pirila PL, Koivuranta KT, Wierenga RK and Hiltunen JK (2002) Organization of the multifunctional enzyme type 1: interaction between N- and C-terminal domains is required for the hydratase-1/isomerase activity. *Biochem J* **367**, 433–441.
39 Onwukwe GU, Koski MK, Pihko P, Schmitz W and Wierenga RK (2015) Structures of yeast peroxisomal Δ3, Δ2-enoyl-CoA isomerase complexed with acyl-CoA substrate analogues: the importance of hydrogen-bond networks for the reactivity of the catalytic base and the oxyanion hole. *Acta Crystallogr D Biol Crystallogr* **71**, 2178–2191.
40 Onwukwe GU, Kursula P, Koski MK, Schmitz W and Wierenga RK (2015) Human Δ3, Δ2-enoyl-CoA isomerase, type 2: a structural enzymology study on the catalytic role of its ACBP domain and helix-10. *FEBS J* **282**, 746–768.
41 Laurino P, Toth-Petroczy A, Meana-Paneda R, Lin W, Truhlar DG and Tawfik DS (2016) An ancient fingerprint indicates the common ancestry of Rossmann-fold enzymes utilizing different ribose-based cofactors. *PLoS Biol* **14**, e1002396.
42 Wierenga RK, Terpstra P and Hol WG (1986) Prediction of the occurrence of the ADP-binding beta alpha beta-fold in proteins, using an amino acid sequence fingerprint. *J Mol Biol* **187**, 101–107.
43 Anderson KS (1999) Fundamental mechanisms of substrate channeling. *Methods Enzymol* **308**, 111–145.
44 Barends TR, Dunn MF and Schlichting I (2008) Tryptophan synthase, an allosteric molecular factory. *Curr Opin Chem Biol* **12**, 593–600.
45 Lovell SC, Davis IW, Arendall WB 3rd, de Bakker PI, Word JM, Prisant MG, Richardson JS and Richardson DC (2003) Structure validation by Calpha geometry: phi, psi and Cbeta deviation. *Proteins* **50**, 437–450.
46 Waterson RM and Hill RL (1972) Enoyl coenzyme A hydratase (crotonase). Catalytic properties of crotonase and its possible regulatory role in fatty acid oxidation. *J Biol Chem* **247**, 5258–5265.

Supporting information

Additional Supporting Information may be found online in the supporting information tab for this article:

Fig. S1. The sequence alignment of rat peroxisomal MFE1 (rpMFE1) and human mitochondrial HAD (HsHAD).

Fig. S2. The 2Fo-Fc electron density omit maps defining the mode of binding of the active site ligands.

Fig. S3. Comparison of the mode of binding of AcAc-CoA to the hydratase active sites of MFE1 and the monofunctional hydratase.

Fig. S4. The structure of the HAD part of MFE1 in complex with NAD^+.

Fig. S5. Comparison of the mode of binding of NAD^+ to the NAD-binding domains of the binary complexes of MFE1 and HsHAD.

Video S1. The conformational flexibility of MFE1.